

Data-Dependent Generalization Bounds for Parameterized Quantum Models Under Noise

Bikram Khanal^{ID} and Pablo Rivas^{ID}

School of Engineering & Computer Science, Baylor University, One Bear Place, Waco, 76798, TX, USA.

*Corresponding author(s). E-mail(s): pablo_rivas@baylor.com;
Contributing authors: bikram_khanal1@baylor.edu;

Abstract

Quantum machine learning offers a transformative approach to solving complex problems, but the inherent noise hinders its practical implementation in near-term quantum devices. This obstacle makes it challenging to understand the generalization capabilities of quantum circuit models. Designing robust quantum machine learning models under noise requires a principled understanding of complexity and generalization, extending beyond classical capacity measures. This study investigates the generalization properties of parameterized quantum machine learning models under the influence of noise. We present a data-dependent generalization bound grounded in the quantum Fisher information matrix. We leverage statistical learning theory to relate the parameter space volumes and training sizes to estimate the generalization capability of the trained model. By integrating local parameter neighborhoods and effective dimensions defined through quantum Fisher information matrix eigenvalues, we provide a structured characterization of complexity in quantum models. We analyze the tightness of the bound and discuss the trade-off between model expressiveness and generalization performance.

Keywords: Quantum Machine Learning, Generalization Bound, Noise Channel, NISQ

1 Introduction

Quantum machine learning (QML) holds the promise of revolutionizing data analysis by leveraging quantum mechanical principles to enhance computational efficiency and model expressivity [1–3]. While still in its early stages [4–6], QML has shown potential

advantages over classical machine learning in certain tasks, such as classification [7, 8], regression [9], and clustering [10]. A crucial aspect of any machine learning model, including QML models, is its ability to generalize. Generalization refers to a model’s capacity to perform well on unseen data [11–13]. Generalization bounds provide theoretical guarantees on the performance of a model on new data, and they play a vital role in ensuring the reliability and robustness of machine learning models [14–16].

One of the prominent questions in QML is understanding how noise affects the generalization ability of the models [17–19]. Generalization bounds are typically derived by bounding a complexity measure of the hypothesis class employed for learning [19]. These complexity measures, such as Rademacher complexity, VC dimension, and metric entropy, quantify the expressiveness or capacity of the model class. Generalization bounds are particularly important due to the inherent challenges posed by quantum systems, especially in the Noisy Intermediate-Scale Quantum (NISQ) era [6, 18–22]. NISQ devices are characterized by limited qubit coherence times, gate fidelities, and susceptibility to noise, which can significantly impact the performance and reliability of QML models. Several studies have investigated generalization bounds for QML [6, 15, 17–19, 21–26], exploring various approaches such as uniform bounds, margin-based bounds, and stability analysis [27]. These studies have provided valuable insights into the factors influencing the generalization capabilities of QML models, including the architecture of quantum neural networks (QNNs), data encoding strategies, and the choice of optimization algorithms. Furthermore, research has explored the impact of noise on QML [4, 28–30], highlighting the challenges of maintaining model accuracy in the presence of noise. These noises, arising from various sources like decoherence [31], gate errors, and other quantum phenomena, pose a formidable challenge to developing QML models that can reliably learn and generalize from data. Although strategies for mitigating noise [32, 33, 33, 34], have been proposed to improve the performance of QML models, most existing research [17–19, 21, 35–38] on QML generalization bounds focuses on idealized, noise-free quantum computers. Researchers have also explored the QML model’s generalization capability in the context of quantum kernels [37, 39, 40]. However, these bounds are often tailored to the specific algorithmic technique or the problem at hand. Hence, a comprehensive understanding of how noise affects the generalization performance of QML models is still lacking. This gap is particularly critical in the NISQ era, where noise is unavoidable and can severely limit the practical applicability of QML algorithms. In fact, some studies [4, 29, 30, 36, 40, 41] suggest that quantum noisy channels can significantly hinder the capabilities of QML, potentially affecting their practical applications. We note that the generalization capabilities of the quantum neural network models may suffer from the barren plateau problem [29, 42–47] and quantum kernel methods from exponential concentration [41]. Please note that the training-induced noise is different from the inherent noise in the quantum devices and is not considered in this work.

In this work, we address this gap by investigating the generalization bound for QML under a noisy channel. Specifically, we consider a scenario where a QML model is trained on a noisy quantum system, and the goal is to establish a bound on its generalization error in the presence of noise. We achieve this goal by leveraging the quantum Fisher information-derived metrics, parameter space volume, and training

sample size into a quantifiable measure of complexity in noisy QML models and derive the generalization bound for near-term QML models. Our approach interprets complexity as a controllable quantity rather than an abstract or unbounded factor. The work refines global bounds by considering local parameter neighborhoods, effective dimensions defined through quantum Fisher information matrix (QFIM) eigenvalues, and conditions that stabilize complexity growth under noise. As a consequence, our work bridges abstract theoretical concepts and the operational needs of quantum learning architectures. The contribution lies not in proposing new computational primitives, but in producing a rigorous theoretical structure that uses geometric principles to inform model design. Rather than treating all parameters equally through our approach, it becomes clear that parameter directions differ in their contribution to predictive performance, making geometric considerations not just aesthetic choices but practical necessities.

The remainder of this paper proceeds as follows. The next section presents a preliminary background in machine learning and the quantum machine with the formal setup of binary classification learning problems. We discuss classical and quantum Fisher information briefly in section 3, and the effective dimension in section 3. Section 5 proposes the generalization bound and corollaries followed by a local refinement. A subsequent section 6 discusses empirical validation through numerical experiments, confirming the agreement with theoretical predictions. We discuss these results in a broader context in section 8 and summarize key contributions in section 9. Appendix 9 provides detail in the mathematical derivation of the proposed bound with the necessary background.

2 Preliminary Definitions

We begin by discussing the fundamental concepts of learning from data and extending them to the QML framework. This discussion is based on the supervised learning setting. Readers who are already familiar with the field may skip the following two subsections. For those seeking a deeper understanding, we recommend the books by [12, 13] for classical learning theory, and the books by [1, 48] for QML and quantum information background.

2.1 Supervised Learning

In supervised learning, we are given the input space \mathcal{X} and the output space \mathcal{Y} . Let P be the joint probability distribution over $\mathcal{X} \times \mathcal{Y}$ and $D = \{(x_i, y_i)\}_{i=1}^N$ be a dataset of N i.i.d samples drawn from P . The goal of supervised learning is to learn a function $f : \mathcal{X} \rightarrow \mathcal{Y}$ that maps input to output. Given a training dataset D , the learning algorithm \mathcal{A} selects the best function h from a hypothesis class \mathcal{H} . Usually, the elements of \mathcal{H} are parameterized by a vector of parameters $\theta \in \Theta$, where $\Theta \subset \mathbb{R}^d$ is a parameter space of $d \in \mathbb{N}$ dimension. We may also refer to h as h_θ to emphasize the dependence on the parameters and define the hypothesis class as $\mathcal{H} = \{h_\theta : \theta \in \mathbb{R}^d\}$. Please note that h and f are used interchangeably as hypotheses in the context of learning and this might be exhibited in our manuscript too.

Given two approximations $h_1, h_2 \in \mathcal{H}$ how do we decide which one is better? One way to do that is to define a loss function $l : \mathcal{Y} \times \mathcal{X} \rightarrow \mathbb{R}$. The loss function measures the difference between the predicted output $\hat{y} \in \mathbb{R}$ and the true output $y \in \mathcal{Y}$. The learning algorithm aims to find h that minimizes the expected loss (or expected risk) defined as:

$$R(h) = \mathbb{E}_{(x,y) \sim P}[l(y, h(x))]. \quad (1)$$

The expected risk is the average loss over all possible inputs and outputs. Therefore, the goal is to find a function h such that $l(h)$ is as small as possible. In practice, we do not have access to the true distribution P and hence it is often challenging to compute the expected risk. Instead, we compute the empirical risk, and try to minimize it, also referred to as the empirical risk minimization (ERM) principle. The empirical risk is defined as:

$$\hat{R}(h) = \frac{1}{N} \sum_{i=1}^N l(y_i, h(x_i)). \quad (2)$$

A central goal of machine learning is to understand how well the empirical risk approximates the expected risk [11–13, 49]. The difference between the empirical risk and the expected risk is known as the generalization error. The generalization error quantifies how well the model generalizes from the training data to unseen data. A model with low generalization error is said to generalize well, while a model with high generalization error suggests poor generalization. Generalization error is typically of the form:

$$\text{GenError} = R(h) - \hat{R}(h). \quad (3)$$

One of the important uses of generalization error is to provide a bound on the expected risk of the model. We can use the probability to bound the generalization error as:

$$\Pr \left[\sup_{h \in \mathcal{H}} \left| \hat{R}(h) - R(h) \right| \leq \epsilon \right] \geq 1 - \delta, \quad (4)$$

where $\Pr[\cdot]$ denotes the probability measure, \sup is the supremum, ϵ is the error tolerance, and δ is the confidence level. The uniform convergence bound given by equation (4) implies that with probability at least $1 - \delta$, the empirical risk of the best hypothesis in the hypothesis class is close to the expected risk. We can use the uniform convergence bound approach to provide a bound on the generalization error, i.e. generalization bound. The generalization bound provides a guarantee of how well the model generalizes to unseen data [50, 51]. Generalization bound is typically of the form:

$$R(h) \leq \hat{R}(h) + \text{complexity term}, \quad (5)$$

where the complexity term is often a function of the \mathcal{H} and N . Complexity measure depends on P over $\mathcal{X} \times \mathcal{Y}$ and if P is easy to learn, the complexity term will be small. In other words, if we are to find the model with the low complexity term, we can expect the model to generalize well [52, 53].

Alternatively, instead of getting a bound on the probability of the generalization error, we can obtain an upper bound in generalization error expectations instead. i.e.,

we can bound the expected generalization error as:

$$\mathbb{E}_D \left[\sup_{h \in \mathcal{H}} \left| \hat{R}(h) - R(h) \right| \right] \leq \text{complexity term}, \quad (6)$$

where the expectation is taken over the training dataset D . In this work, we focus on the expected generalization error bound and provide a bound on the expected generalization error for quantum machine learning models in noisy environments. Before proceeding, we briefly discuss the quantum machine learning framework.

2.2 Quantum Machine Learning

Consider a binary classification setting with $\mathcal{X} \subset \mathbb{R}^m$ and $\mathcal{Y} = \{-1, +1\}$. Let \mathcal{H}_s be a Hilbert space associated with an n -qubit quantum system, so $\dim(\mathcal{H}_s) = 2^n$. Let $\phi : \mathcal{X} \rightarrow \mathcal{H}_s$ be a feature map that encodes a classical input $x \in \mathcal{X}$ into a state $|\phi(x)\rangle \in \mathcal{H}_s$. Consider $n_\phi \leq n$ as the number of qubits used to encode $|\phi(x)\rangle$. Define an initial state:

$$|\psi(x)\rangle = |\phi(x)\rangle \otimes |0\rangle^{\otimes(n-n_\phi)}. \quad (7)$$

A parameterized quantum circuit (PQC) [8, 54] with parameters $\theta = (\theta_1, \dots, \theta_L)$ acts on $|\psi(x)\rangle$ via a unitary $U(\theta) = \prod_{k=1}^L U_k(\theta_k)$, where each $U_k(\theta_k)$ is a parameterized unitary. The resulting state is:

$$|\psi_\theta(x)\rangle = U(\theta) |\psi(x)\rangle. \quad (8)$$

For pure states, the density matrix representation is:

$$\rho_\theta(x) = |\psi_\theta(x)\rangle \langle \psi_\theta(x)|. \quad (9)$$

To extract a classical prediction, apply a two-outcome measurement described by a POVM $\{M_{+1}, M_{-1}\}$ on the first qubit. Let $M_{+1} = |0\rangle \langle 0| \otimes I$ and $M_{-1} = |1\rangle \langle 1| \otimes I$, where I is the identity operator on the remaining $n-1$ qubits. The probability of obtaining label $y \in \{+1, -1\}$ for input x is:

$$p(y|x; \theta) = \text{Tr} [M_y \rho_\theta(x)]. \quad (10)$$

Next, we discuss how does the probability of measurement outcomes changes under a noisy quantum channel.

2.3 Incorporating a Noisy Quantum Channel

Consider a noisy quantum channel \mathcal{N} , a completely positive trace-preserving (CPTP) map acting on density operators. The state after the noisy channel is:

$$\tilde{\rho}_\theta(x) = \mathcal{N}(\rho_\theta(x)). \quad (11)$$

Under the noisy channel \mathcal{N} , the measured probabilities become:

$$\tilde{p}(y|x;\theta) = \text{Tr}[M_y \tilde{\rho}\theta(x)] = \text{Tr}[M_y \mathcal{N}(\rho\theta(x))]. \quad (12)$$

For certain noise channels and measurement bases, it can be assumed that the noisy probability $\tilde{p}(y|x;\theta)$ relates to the noiseless probability $p(y|x;\theta)$ through a differentiable function $\eta : [0, 1] \rightarrow (0, 1]$:

$$\tilde{p}(y|x;\theta) = \eta(p(y|x;\theta)), \quad (13)$$

with η continuous in the noise rate and $\eta(0) = 1$ [55, 56]. Such a simplification holds, for example, when the noise operators commute with the measurement operators, as is the case with a depolarizing channel acting on states measured in the computational basis [48, 57–59].

Incorporating noise modifies the sensitivity of output probabilities with respect to variations in θ . Analyzing the behavior of $\tilde{p}(y|x;\theta)$ as a function of θ under noise is crucial for understanding the trainability and generalization properties of quantum machine learning models. This sensitivity can be quantified through the Fisher information matrices, both classical and quantum, which serve as fundamental tools for analyzing parameter distinguishability and generalization in the presence of noise [60–63].

3 Fisher Information

From a machine learning perspective, the Fisher information measures the sensitivity of the output label distribution with respect to changes in model parameters [64–67]. Higher Fisher information indicates that the parameters θ carry more information about the output label y , thereby enabling more precise parameter estimation and potentially improving learnability. In a quantum machine learning setting, we must consider both classical and quantum notions of Fisher information to fully capture the role of quantum states and measurements.

3.1 Classical Fisher Information

Consider a parameterized probability distribution $p(y|x;\theta)$, where $y \in \mathcal{Y}$ denotes the label and $\theta = (\theta_1, \dots, \theta_d)$ are the model parameters. The classical Fisher information matrix (FIM) is defined as:

$$\mathcal{F}(\theta)_{ij} = \sum_{y \in \mathcal{Y}} p(y|x;\theta) \left(\frac{\partial \ln p(y|x;\theta)}{\partial \theta_i} \right) \left(\frac{\partial \ln p(y|x;\theta)}{\partial \theta_j} \right). \quad (14)$$

Equivalently, this can be written as:

$$\mathcal{F}(\theta)_{ij} = \sum_{y \in \mathcal{Y}} \frac{1}{p(y|x;\theta)} \left(\frac{\partial p(y|x;\theta)}{\partial \theta_i} \right) \left(\frac{\partial p(y|x;\theta)}{\partial \theta_j} \right). \quad (15)$$

The classical FIM quantifies how sensitive the observed label distribution is to small perturbations of the parameters. PQC measurement outcomes form the probability distribution. However, in the near-term there is the exponential growth of potential measurement outcomes as the number of quantum bits increases [68]. This means, there might be many measurement outcomes, although with minimal probability, that never appear causing instability in classical Fisher information matrix computation [63, 65].

3.1.1 Fisher Information Under a Noisy Channel

When a noisy quantum channel \mathcal{N} acts on the underlying quantum state, the probability distribution $p(y|x; \theta)$ is replaced by $\tilde{p}(y|x; \theta)$ defined in Eq. (12). The corresponding noisy classical FIM becomes:

$$\tilde{\mathcal{F}}(\theta)_{ij} = \sum_{y \in \mathcal{Y}} \frac{1}{\tilde{p}(y|x; \theta)} \left(\frac{\partial \tilde{p}(y|x; \theta)}{\partial \theta_i} \right) \left(\frac{\partial \tilde{p}(y|x; \theta)}{\partial \theta_j} \right). \quad (16)$$

Using the relationship in Eq.(13) and the chain rule, we have:

$$\frac{\partial \tilde{p}(y|x; \theta)}{\partial \theta_i} = \eta' (p(y|x; \theta)) \frac{\partial p(y|x; \theta)}{\partial \theta_i}, \quad (17)$$

where η and η' characterize the noise-induced transformation of the probabilities. Substituting Eq.(17) into Eq. (16), we get:

$$\tilde{\mathcal{F}}(\theta)_{ij} = \sum_{y \in \mathcal{Y}} \frac{[\eta'(p(y|x; \theta))]^2}{\eta(p(y|x; \theta))} \left(\frac{\partial p(y|x; \theta)}{\partial \theta_i} \right) \left(\frac{\partial p(y|x; \theta)}{\partial \theta_j} \right). \quad (18)$$

This expression shows that the noisy classical FIM is the noiseless FIM scaled by factors depending on η and η' . If $\eta' \approx 1$, noise minimally affects gradients. If $\eta' > 1$, the model is more sensitive to parameter changes, possibly improving short-term learnability but risking overfitting. If $\eta' < 1$, the parameter sensitivity is suppressed, potentially resulting in slower training and higher bias. These dynamics reflect the interplay between noise and trainability in quantum machine learning models.

The classical FIM considered so far treats measurement outcomes as classical data. While this is sufficient for fixed measurements, it does not exploit the full quantum nature of the underlying states. To fully characterize parameter sensitivity at the quantum level, one must turn to the Quantum Fisher Information (QFI), which provides a more fundamental and measurement-independent measure of distinguishability of quantum states [69–71].

3.2 Quantum Fisher Information

The Quantum Fisher Information (QFI) [63, 65, 70, 72] generalizes the concept of Fisher information to the quantum domain. Instead of fixing a particular measurement, the QFI considers the most informative measurement possible. This makes the

QFI a fundamental limit on parameter precision achievable with an optimal choice of measurement.

3.2.1 Ideal (Pure) States

For a single-parameter family of pure states $|\psi(\theta)\rangle$, the QFI is given by [73, 74]:

$$F_Q(\theta) = 4 [\langle \partial_\theta \psi(\theta) | \partial_\theta \psi(\theta) \rangle - |\langle \psi(\theta) | \partial_\theta \psi(\theta) \rangle|^2]. \quad (19)$$

If $|\psi(\theta)\rangle = e^{-iG\theta} |\psi(0)\rangle$ for some Hermitian generator G , this simplifies to:

$$F_Q(\theta) = 4 \langle \psi(0) | (\Delta G)^2 | \psi(0) \rangle, \quad (20)$$

where $(\Delta G)^2 = G^2 - \langle G \rangle^2$.

3.2.2 Noisy (Mixed) States

For a mixed state $\rho(\theta)$, the QFI is defined using the Symmetric Logarithmic Derivative (SLD) L_θ , which satisfies:

$$\frac{\partial \rho(\theta)}{\partial \theta} = \frac{1}{2} (L_\theta \rho(\theta) + \rho(\theta) L_\theta). \quad (21)$$

The QFI is then:

$$F_Q(\theta) = \text{Tr}[\rho(\theta) L_\theta^2]. \quad (22)$$

If $\rho(\theta) = \sum_i \lambda_i(\theta) |\psi_i(\theta)\rangle \langle \psi_i(\theta)|$ is the spectral decomposition, one can write [74]:

$$L_\theta = \sum_{i,j} \frac{2}{\lambda_i(\theta) + \lambda_j(\theta)} \langle \psi_i(\theta) | \partial_\theta \rho(\theta) | \psi_j(\theta) \rangle |\psi_i(\theta)\rangle \langle \psi_j(\theta)|. \quad (23)$$

For multiple parameters $\theta = (\theta_1, \dots, \theta_d)$, the QFI generalizes to a matrix known as the Quantum Fisher Information Matrix (QFIM). The QFIM's elements can be derived from the SLDs corresponding to each parameter, and it encodes the distinguishability of $\rho(\theta)$ in all parameter directions. This multi-parameter QFIM reduces to the single-parameter QFI if we focus on one parameter at a time.

3.3 Relationship between Classical and Quantum Fisher Information

Consider a measurement described by a POVM $\{M_x\}$, where the probability of obtaining outcome x is $p(x|\theta) = \text{Tr}[\rho(\theta) M_x]$. The corresponding Classical Fisher Information (CFI) is:

$$F_C(\theta) = \sum_x p(x|\theta) \left(\frac{\partial}{\partial \theta} \ln p(x|\theta) \right)^2. \quad (24)$$

The Quantum Cramér-Rao bound states:

$$\text{Var}(\hat{\theta}) \geq \frac{1}{MF_Q(\theta)}, \quad (25)$$

where $\hat{\theta}$ is an unbiased estimator, and M is the number of experiments. Since the QFI represents the maximal information obtainable over all possible measurements, we have:

$$F_C(\theta) \leq F_Q(\theta), \quad (26)$$

with equality when the chosen POVM attains the quantum limit.

This relationship shows that the QFI provides a fundamental upper bound on the precision achievable by any measurement scheme, making it a key tool in quantum parameter estimation [63]. Classical Fisher information depends on the chosen measurement, whereas quantum Fisher information is measurement-independent and sets the ultimate precision limit.

The concepts of classical and quantum Fisher information, and their interplay, form the foundation for defining complexity measures such as the effective dimension of a parameter space. The next section introduces the effective dimension and its role in understanding generalization in quantum machine learning models.

4 Effective Dimension

The notion of effective dimension [60, 75, 76] provides a quantitative measure of the intrinsic complexity associated with a set of parameters used to describe a quantum system or a learning model. In contrast to the raw dimension d of the parameter space, which simply counts the number of free parameters, the effective dimension focuses on how sensitively these parameters influence observable outcomes. Parameters that do not appreciably affect the system's distinguishability are effectively inert, and thus, the model's complexity can be characterized in terms of a smaller dimension than the naive counting argument might suggest.

In the context of quantum machine learning and metrology, the QFIM plays a central role in defining the effective dimension. The QFIM,

$$F_{ij}(\theta) = 4, \text{Re} [\langle \partial_i \psi(\theta) | \partial_j \psi(\theta) \rangle - \langle \partial_i \psi(\theta) | \psi(\theta) \rangle \langle \psi(\theta) | \partial_j \psi(\theta) \rangle], \quad (27)$$

encodes how sensitively the quantum state $|\psi(\theta)\rangle$ changes in each parameter direction θ_i . Although the QFIM is defined for pure states as above, analogous formulations exist for mixed states (details in 3.2.2, and [63]), ensuring its general applicability. As long as the state remains full rank (or can be approximated by one), the QFIM robustly quantifies the parameter dependence of state distinguishability.

To isolate the intrinsic parameter dependence from differences in the overall scale of the information, one can define the effective dimension as:

$$d_{\text{eff}} = \max_{\theta \in \Theta} \text{rank } F(\theta) \quad (28)$$

When all directions in parameter space contribute equally and significantly, d_{eff} approaches the full parameter dimension d . However, in many scenarios, the spectrum of the QFIM is highly non-uniform: a few eigenvalues may dominate, corresponding to directions in which changes in θ lead to large, easily distinguishable shifts in the state, while other eigenvalues may be vanishingly small, reflecting directions that barely affect the state’s geometry. In such a situation, $d_{\text{eff}} \ll d$, indicating that the system effectively behaves as if it is parameterized by fewer “active” directions.

An alternative, and often practically convenient, approximation emerges by considering the eigenvalues of the (unnormalized) QFIM, F . Under the assumption that the trace $\sum_i \lambda_i$ and the sum of squares $\sum_i \lambda_i^2$ capture the leading structure of the spectrum, one may approximate:

$$d_{\text{eff}} \approx \frac{\left(\sum_{i=1}^d \lambda_i\right)^2}{\sum_{i=1}^d \lambda_i^2}. \quad (29)$$

This approximation relates the effective dimension to a ratio reminiscent of the inverse participation ratio used in other fields to measure how “concentrated” a distribution is. A sharp spectral concentration—where one or a few eigenvalues are significantly larger than the rest—yields a lower effective dimension, whereas a more uniform distribution of eigenvalues yields a higher effective dimension closer to d .

The effective dimension thus integrates the geometric properties of the quantum state’s manifold with respect to its parameters. It discerns how many directions in parameter space genuinely alter the model’s predictions in a statistically distinguishable way. Such a measure informs model selection procedures, since a large gap between d and d_{eff} suggests that certain parameters may not improve the model’s descriptive power. In quantum metrology, a high effective dimension implies a broad capacity for precise multiparameter estimation, while a low effective dimension indicates that the sensitivity to variations is restricted to a few principal directions.

By enabling us to move beyond simplistic dimensional counting and instead focus on the meaningful parameter degrees of freedom, the effective dimension offers insight into the complexity and scalability of quantum machine learning models. It serves as a valuable tool for understanding the interplay between parameterization, state distinguishability, and achievable precision in both learning and estimation tasks.

5 Generalization bound

In this section, we describe the main contribution of our work by providing a generalization bound for quantum machine learning models in noisy environments. Building upon statistical learning theory [11, 77] and quantum information theory [48], we prove our main result in Appendix [B.2]:

Theorem 5.1. *[Generalization Bound for Parameterized Quantum Models] Let $d, N \in \mathbb{N}$ and $\delta \in [0, 1)$. Consider a d -dimensional parameter space $\Theta \subset \mathbb{R}^d$ a class of quantum machine learning model functions $\mathcal{F}_\Theta = \{f_{\theta,p} : \theta \in \Theta\}$ where each model output under a noisy channel with noise parameter $p \in [0, 1)$ is given*

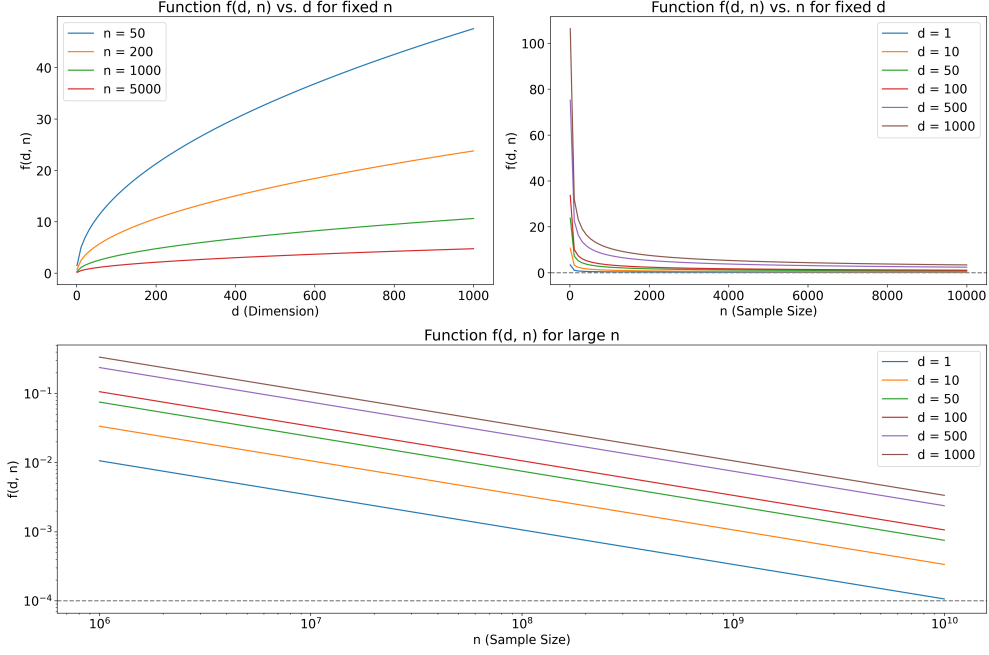


Fig. 1: Rademacher Complexity $f(d, n)$ as a function of the number of samples n and the dimensionality d . Please note we have applied the log scaling on both axes for the third figure (second row) for better visualization.

by: $f_{\theta, p}(x) = \eta(p)f_{\theta}(x)$, with $\eta : [0, 1] \rightarrow (0, \infty)$ a perturbation function satisfying $\eta(0) = 1$. Assume the following:

- **Loss Function:** The loss $l : \mathcal{Y} \times \mathbb{R} \rightarrow [0, 1]$ is Lipschitz continuous in its second argument with Lipschitz constant $L > 0$.
- **Perturbed model bounded gradient:** The gradient of the perturbed model $f_{\theta, p}(x)$ w.r.t θ is bounded by the Lipschitz constant L_f^p : $\|\nabla_{\theta} f_{\theta, p}(x)\| \leq L_f^p, \forall x \in \mathcal{X}, \theta \in \Theta$.
- **FIM Lower Bound:** Let $\mathcal{F}(\theta)$ denote the quantum Fisher Information Matrix associated with the model. Suppose there exists $m > 0$ such that:

$$\sqrt{\det(\mathcal{F}(\theta))} \geq m > 0, \quad \forall \theta \in \Theta.$$

Let V_{Θ} be the volume of the parameter space Θ and define:

$$C' = \log V_{\Theta} - \log V_d - \log m + d \log L_f^p,$$

where $V_d = \frac{\pi^{\frac{d}{2}}}{\Gamma(\frac{d}{2}+1)}$ is the volume of a unit ball in \mathbb{R}^d , and $\Gamma(\cdot)$ is the gamma function. Then, for any $\delta > 0$, with probability at least $1 - \delta$ over the random draw of an i.i.d. training set $D = \{(x_i, y_i)\}_{i=1}^N \sim P$, the following generalization bound holds uniformly

d	k(d)	N	Third Term, $\delta = 0.005$
1	2.72	8	0.99
10	3.49	13	0.60
100	10.10	102	0.07
1000	31.65	1002	0.01
10000	100.01	10002	0.00
50000	223.61	50002	0.00
100000	316.23	100002	0.00

Table 1: Estimated generalization error scaling for increasing model dimensionality. Each column shows the parameter dimension d , a complexity measure $k(d)$, the approximate sample size N required to reduce complexity-driven overhead, and the resulting complexity term of the bound. Higher dimensionality increases complexity, yet the growth is modest; with sufficient samples, even very high-dimensional models can achieve negligible complexity contributions.

for all $\theta \in \Theta$:

$$R(\theta) \leq \hat{R}_N(\theta) + \frac{12\sqrt{\pi d} \exp(C'/d)}{\sqrt{N}} + 3\sqrt{\frac{\log(2/\delta)}{2N}}. \quad (30)$$

where $R(\theta) = \mathbb{E}_{(x,y) \sim P}[l(y, f_{\theta,p}(x))]$ is the expected risk and $\hat{R}_N(\theta) = \frac{1}{N} \sum_{i=1}^N l(y_i, f_{\theta,p}(x_i))$ is the empirical risk.

Theorem 5.1 provides a data-dependent generalization bound for parameterized quantum models under noise. It reveals how sample size N , parameter dimension d , and model complexity interplay. For large N , the third term $\sim \sqrt{\frac{\log(2/\delta)}{N}}$ becomes negligible. Consequently, the dominant complexity term $\frac{12\sqrt{\pi d} \exp(C'/d)}{\sqrt{N}}$ and the empirical risk $\hat{R}_N(\theta)$ determine the model's capacity to generalize.

As d grows large, $\exp(C'/d) \rightarrow 1$, so the complexity scales approximately as \sqrt{d} . Intuitively, having more parameters can increase complexity, yet the $\frac{1}{\sqrt{N}}$ factor ensures that as N grows, the model complexity effectively diminishes, improving generalization. Nevertheless, if the dataset is small, increasing the dimension d can make generalization more challenging.

This bound also emphasizes that, for any fixed d , the complexity term decreases as N increases, suggesting that, in the limit $N \rightarrow \infty$, the model's generalization error can be made arbitrarily small. However, as shown in Fig. 1 for any finite N , there is always a non-zero complexity term. Thus, even though we may achieve empirical risk close to zero, the interplay of dimension and sample size ensures that perfect generalization is not guaranteed.

To gain further insight, consider:

$$k(d) = \sqrt{d} \exp\left(\frac{C'}{d}\right).$$

For large d , $k(d)$ grows slower than linearly but still increases with d . Roughly, one requires on the order of $k(d)^2$ data points to push the complexity-driven error below a threshold of $12\sqrt{\pi}$. From table 1 it is apparent that by appropriately increasing the number of training samples N , one can significantly push down the complexity term, making it nearly minimal for large data sets. The practical challenge of generalizing with high-dimensional parameter spaces can be tackled by ensuring adequate sample sizes. This aligns with the well-established notion in machine learning that more data leads towards better generalization. Ultimately, while high-dimensional models might start off more complex, the capacity to temper that complexity with larger datasets allows such models to remain viable, reinforcing that sufficient data can offset the dimensional burden.

The global bound in Theorem 5.1 considers the worst-case scenario over the entire parameter space Θ . In practice, after training converges, the learned parameter $\hat{\theta}$ may reside in a much smaller, effectively low-complexity region. This motivates local bounds that yield tighter guarantees.

Corollary 5.2. *[Local Generalization Bound] Let the conditions of Theorem 5.1 hold. Suppose after training, $\hat{\theta}$ is a solution, and consider a local neighborhood $\Theta_{loc} \subset \Theta$ around $\hat{\theta}$ as $\Theta_{loc} := \{\theta \in \Theta : \|\theta - \hat{\theta}\| \leq \delta\}$ where $\delta > 0$ but up to global limits. Assume within Θ_{loc} :*

- The Fisher Information Matrix remains well-conditioned: $\sqrt{\det(\mathcal{F}(\theta))} \geq m_{loc} > 0$.
- The gradients of the perturbed model are bounded locally by $L_{f,loc}^p$.

Define: $C_{loc} = \log(V_{\Theta_{loc}}) - \log(V_d) - \log(m_{loc}) + d \log(L_{f,loc}^p)$, where $V_{\Theta_{loc}}$ is the volume of the local region. Then, with probability at least $1 - \delta$, for all $\theta \in \Theta_{loc}$:

$$R(\theta) \leq \hat{R}N(\theta) + \frac{12\sqrt{\pi d} \exp(C_{loc}/d)}{\sqrt{N}} + 3\sqrt{\frac{\log(2/\delta)}{2N}}. \quad (31)$$

Proof. This follows from Theorem 5.1 by restricting the parameter space to the smaller, better-conditioned subset Θ_{loc} . Replacing global parameters m and L_f^p with their local counterparts m_{loc} and $L_{f,loc}^p$, and using $V_{\Theta_{loc}}$ in place of V_{Θ} , leads to the stated local bound. The same Rademacher complexity and covering number arguments apply but over a reduced search space, thereby potentially tightening the bound. \square

Corollary 5.2 shows that if training converges to a region where parameters vary less and the Fisher information remains stable, the complexity term decreases. This improved local conditioning can yield sharper generalization guarantees.

Corollary 5.3. *[Effective Dimension and QFIM] Let $\mathcal{F}(\theta)$ denote the QFIM and assume: $\sqrt{\det(\mathcal{F}(\theta))} \geq m > 0$, $\forall \theta \in \Theta$. Suppose $\lambda_1(\theta) \geq \dots \geq \lambda_d(\theta) > 0$ are the eigenvalues of $\mathcal{F}(\theta)$. For a threshold $\alpha > 0$, define the effective dimension: $d_{\text{eff}}(\alpha) = \max\{r \leq d : \lambda_r(\theta) \geq \alpha, \forall \theta \in \Theta\}$. Then, applying the reasoning of Corollary 5.2 to an effective dimension setting, we obtain with probability at least $1 - \delta$:*

$$R(\theta) \leq \hat{R}N(\theta) + \frac{12\sqrt{\pi d_{\text{eff}}(\alpha)} \exp(C_{loc}/d_{\text{eff}}(\alpha))}{\sqrt{N}} + 3\sqrt{\frac{\log(2/\delta)}{2N}}. \quad (32)$$

Proof. By focusing on the subspace where the QFIM eigenvalues exceed α , we effectively reduce the dimension to $d_{\text{eff}}(\alpha)$. The argument parallels that of Corollary 5.2, simply substituting the effective dimension $d_{\text{eff}}(\alpha)$ and corresponding constants into the main theorem’s complexity estimates. \square

Corollary 5.3 underscores that not all parameters are equally relevant for generalization. The effective dimension $d_{\text{eff}}(\alpha)$ filters out parameter directions that do not significantly affect the state’s distinguishability. This refinement can yield meaningful, dimension-reduced generalization bounds, bridging the gap between theoretical complexity measures and practical model performance.

Overall, Theorem 5.1 and its corollaries highlight how the interplay of sample size N , parameter dimension d , and the geometry of the QFIM govern the generalization capabilities of quantum machine learning models. The effective dimension perspective further refines these insights, guiding the design and training of models that achieve favorable tradeoffs between expressiveness and generalization.

6 Numerical Analysis

We next discuss the numerical analysis performed to validate the proposed theoretical generalization bound. To this end, we designed experiments using a quantum neural network (QNN) with two qubits, evaluated under depolarization noise with rates $p = [0.05, 0.1, 0.5]$. These experiments were performed on two datasets: the Iris dataset (restricted to the first two classes) and the Digits dataset (focused on digits 0 and 1, with features reduced to 8 dimensions). Each experiment was repeated three times to assess the variability of results across multiple runs. This approach allowed us to examine the bound’s tightness, consistency, and applicability under noise conditions relevant to the Noisy Intermediate-Scale Quantum (NISQ) era.

7 Methodology

We focus on empirically validating the proposed generalization bound for a noisy parameterized quantum model. We consider a parameterized quantum model defined by a parameter vector $\theta \in \mathbb{R}^d$, where d represents the number of parameters. For a circuit with n_{layers} layers and n_{qubits} qubits, $d = n_{\text{layers}} \cdot n_{\text{qubits}} \cdot c$, where c is a constant reflecting the number of parameters introduced per qubit per layer. For example, with $n_{\text{qubits}} = 2$ and $n_{\text{layers}} = 2$, and assuming $c = 3$ (e.g., for parameterized single-qubit rotations), we have $d = 12$. To ensure uniform bounds and consistency, we define the global parameter space as $\Theta = [-2\pi, 2\pi]^d$, resulting in a global volume of $(4\pi)^d$.

The model architecture consists of an embedding layer followed by a variational quantum circuit. Classical inputs $\mathbf{x} \in \mathbb{R}^m$ are mapped into quantum states via parameterized single-qubit rotations (e.g., $R_x(x_i)$ or $R_y(x_i)$). Noise is incorporated by inserting depolarizing channels with noise rate $p \in [0, 1)$. The model then becomes $f_{\theta,p}(x) = \eta(p)f_{\theta}(x)$, where $\eta(p)$ scales the expectation value due to noise. This noise has a smoothing effect on the loss landscape, reducing gradient magnitudes and enhancing Fisher Information stability locally.

We train the model by minimizing mean square error loss using a natural gradient descent method. Gradient estimates are obtained using the parameter-shift rule. We trained the model for 20 epochs and a fixed number of runs ($n_{\text{runs}} = 3$) to average the random initialization effects. After training, resulting in trained parameters $\hat{\theta}$, we define a local neighborhood Θ_{loc} around $\hat{\theta}$ to ensure the stability of the quantum FIM. We choose a hypercube for computational simplicity, defined as $\{\theta : \|\theta - \hat{\theta}\|_{\infty} \leq \delta\}$, with a local volume of $(2\delta)^d$. The radius δ is determined by a continuity-based procedure, ensuring that the minimal eigenvalue or determinant-based quantity of the quantum FIM within Θ_{loc} remains above a fraction (e.g., $\alpha = 0.5$) of its value at $\hat{\theta}$. This ensures a stable neighborhood size and minimal conditioning related to the quantum FIM. The value of δ is also constrained to be within the global limits, for example, $\alpha < \delta \leq 2\pi$.

Finally, we compute a local Lipschitz constant $L_{f,\text{loc}}^p$ by sampling gradients within Θ_{loc} and taking the maximum norm. By restricting complexity measures to these stable neighborhoods, the derived local bound becomes tighter and more representative of the model’s actual generalization behavior.

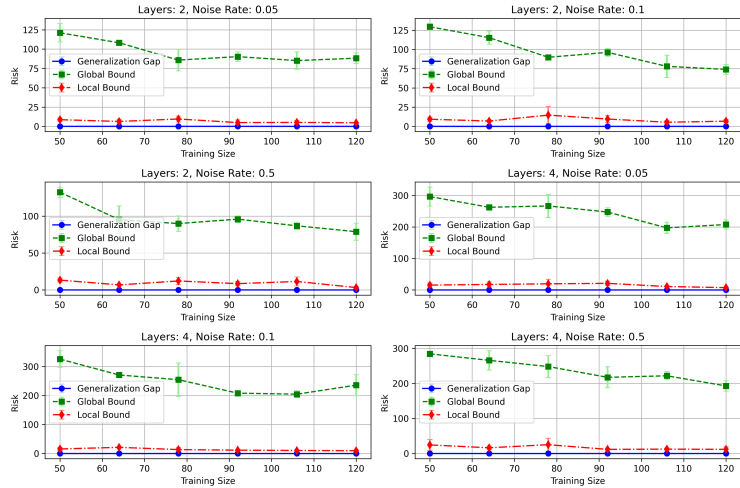
7.1 Result

We evaluated our bounds on the first two classes of iris and $(0, 1)$ class of the MNIST dataset. We performed principal component analysis feature extraction on MNIST to bring it down to 8 features. For each dataset, we plot the generalization gap, the global bound, and the local bound across varying sample sizes, layers, and noise rates which is presented in Fig. 2. The generalization gap remains low across all configurations, and we observe that as the training size increases, the generalization gap tends to decrease or stay close to minimal values. This stability reassures that even in the presence of noise and parameter expansions, the trained quantum models do not overfit severely.

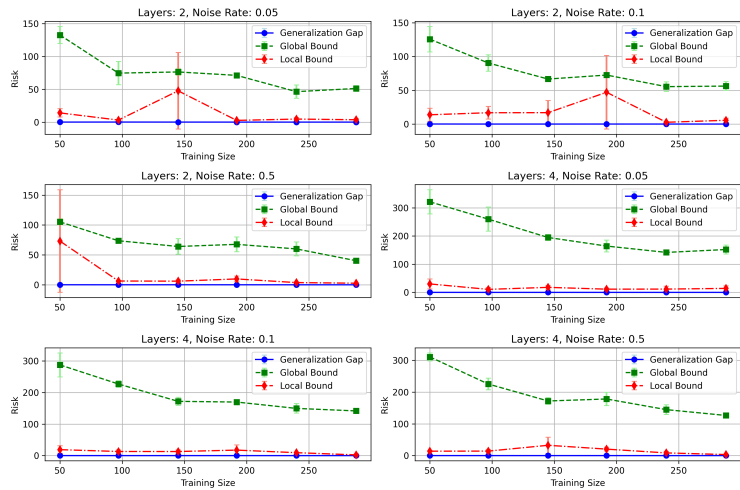
For the Iris dataset, the global bound starts at a high level but decreases as the sample size increases. Yet, it remains significantly above the observed generalization gap, implying a conservative nature typical of worst-case complexity arguments. In contrast, the local bound is consistently closer to the empirical gap, though not perfectly aligned. This improved proximity of the local bound suggests that refining complexity estimates to a stable neighborhood around $\hat{\theta}$ yields more noteworthy upper estimates of risk. The local region’s constraints, influenced by stable Fisher Information conditions and locally computed Lipschitz constants, appear to capture the effective complexity more accurately.

On the Digits dataset the global bound again stands high above the actual gap, but the local bound offers smaller and more stable estimates. Although not perfectly matching the gap, the local bound’s relative closeness and a steadier downward trend as N grows demonstrate that local complexity assessments adapt more naturally to increasing sample sizes. This adaptability supports the argument that local analyses are not merely a heuristic refinement but a necessary step toward a more faithful characterization of generalization in quantum models.

With the Iris dataset, where dimensionality and complexity are relatively small, both global and local bounds descend as training size grows, and the local bound maintains a more moderate scale. The Digits dataset experiments, involving larger



(a) A plot highlighting the global and local bound, and generalization gap on the first two classes of the iris dataset. The local bound provides a tighter estimate of the generalization gap.



(b) A plot on generalization gap, local and global bound on classes (0, 1) on MNIST dataset. Few spikes on the local bound across multiple occurred due to the random initialization of parameters for each run.

Fig. 2: Generalization Bounds for Iris and MNIST Datasets. Each subplot shows the generalization gap, global bound, and local bound as a function of training size for different combinations of layers and noise rates. Error bars represent standard deviation over 3 runs. The local bound's accuracy holds across different model depths, noise levels, and datasets. The result suggests that by focusing on the local geometry around the trained parameters one could get a more realistic and informative assessment of generalization performance

input spaces and potentially more complex variations, show the global bound still inflates above the actual gap. Yet, the local bound remains stable and moves closer to capturing the effective complexity of the learned model. This stability and reduced scale in the local bound, observed across multiple runs and different conditions (varying noise rates and layer counts), supports our theorem 5.1 that local analysis provides a more accurate and data-dependent complexity assessment.

The local bound is not only conceptually appealing but also empirically supported. The differences between global and local complexity trends hint that complexity should not be viewed uniformly across the entire parameter space. Instead, effective complexity is sensitive to the particular region around the trained parameters. Noise, model architecture, and available data samples interact to create a local landscape where complexity-based bounds become more aligned with observed performance. Thus, the local complexity-based generalization analyses may serve as an improved tool for theoretical understanding and practical evaluation of model behavior in realistic, noisy scenarios.

8 Discussion

Our approach of quantifying generalization in quantum machine learning places the geometry of parameterized quantum states at the center of understanding how noise and finite data affect predictive reliability. Parameter space volume, training sample size, and the QFIM emerge as central elements governing complexity. The QFIM, a measure of parameter distinguishability [69, 78, 79], provides insights into how parameter variations relate to model sensitivity, which can inform stability under realistic noise conditions. Classical learning theory often relies on measures such as the VC dimension or the Rademacher complexity [77, 80], yet those concepts lack a direct connection to the geometric and operator-theoretic properties of quantum states. Incorporating the QFIM into the analysis integrates geometric and statistical principles, producing a perspective that relates parameter scaling, data volume, and controlled complexity growth.

Our framework applies across various parameter dimensions and noise levels, and the complexity terms depend on volume measures and gradients within parameter space. The local neighborhood analysis uses the QFIM to focus on parameter regions where complexity remains stable. The effective dimension, derived from QFIM eigenvalues, provides a mechanism for identifying parameter directions that carry predictive significance. This approach extends beyond generic notions of large parameter counts or deep circuits, isolating meaningful subspaces that maintain manageable complexity. Such reasoning relates to efforts linking trainability to structural properties of parameterized circuits [44, 46], introducing a route for shaping model architectures guided by geometric criteria rather than expansions of parameter space.

The data collected from numerical experiments are consistent with the theoretical complexity scaling. Larger parameter dimension increases complexity in a predictable manner related to \sqrt{d} , and larger training sizes correspond to lower complexity-driven errors. These observations connect the theoretical bound directly to practical scenarios. The observed controlled complexity growth suggests that scaling parameter

dimension in quantum models can lead to predictable generalization behavior, provided the interplay between dimension and data volume is managed. The results on effective dimension and local parameter neighborhoods yield tools that may influence the design of parameterized quantum circuits by directing attention toward stable parameter directions and conditions that maintain balanced complexity.

This line of reasoning extends beyond raw measures of expressiveness, linking the predictive reliability of trained quantum models to underlying geometric structures. Conventional arguments about quantum models often revolve around their large state spaces, yet without quantifying how parameter variations interact with data availability and noise. The presence of well-defined complexity bounds clarifies that quantum models can retain consistent behavior as problem sizes grow. Parameters no longer appear as an unstructured collection but as a network of directions differentiated by QFIM eigenvalues. Identifying these directions and controlling them through appropriate training and architectural choices may inform research on QML capacity, optimization strategies, and representational limits [8, 81]. Complexity control is not an abstract ideal; it becomes tangible through geometric metrics and data-driven constraints.

By connecting the QFIM to generalization properties, our analysis relates the structural features of quantum states to the statistical aspects of learning. Instead of relying on heuristic claims or incomplete reasoning, the results rest on a rigorously derived bound and direct empirical support. The outcome is a systematic view of complexity emergence and reduction, guiding both theoretical analysis and practical implementations of quantum learning models.

9 Conclusions

Our work utilizes geometric and statistical principles to relate quantum Fisher information, parameter space volume, and training data to the complexity of learning in noisy quantum models. The proposed bound and numerical results suggest that structured parameter subsets, identified through QFIM eigenvalues, provide a means to ensure stable generalization performance without uncontrolled complexity growth. This work provides a more nuanced understanding of complexity in quantum machine learning by explicitly linking it to the geometry of quantum states and the QFIM, complementing previous studies on expressiveness and capacity. While previous work has explored model capacity and expressiveness in quantum machine learning [2, 7, 9, 82, 83], this work introduces a framework that directly connects parameter-dependent complexity to the tangible geometry of quantum states via the QFIM.

From the perspective of the work proposed here, complexity emerges as a controllable quantity, motivating future research that refines parameter selection or training protocols to preserve stability in large-scale or resource-constrained learning tasks. Work on adaptive circuit structures, informed by local QFIM-based criteria, may help identify directions that maintain manageable complexity while improving representational fidelity. The proposed theorem incorporates noise effects through a general perturbation function, ensuring that performance remains stable under a

broad range of conditions. Investigating individual or combined noise channels, diverse parametrization, or dynamic processes offers avenues for refining model architectures and optimizing strategies to further enhance adaptability and scalability within the QML context. The insights presented here may stimulate investigations into hybrid quantum-classical designs and application-tailored model architectures, paving the way for more robust, scalable, and interpretable quantum machine learning methods.

Declarations

Funding. Part of this work was performed while P.R. was funded by the National Science Foundation under Grant Nos. 2136961, and 2210091, and 1905043. The views expressed herein are solely those of the author(s) and do not necessarily reflect those of the National Science Foundation.

Conflict of interest. The authors have no relevant financial or non-financial interests to disclose.

Availability of data and materials. Data sharing does not apply to this article as no datasets were generated or analyzed during the current study. This article is a systematic literature review, and as such, it synthesizes and analyzes information from previously published literature.

Appendix A

A.1 Parameter Space Geometry

In the main text, we introduced the Fisher information matrix (FIM) $\mathcal{F}(\theta)$ as a Riemannian metric on the parameter space $\Theta \subset \mathbb{R}^d$. This induces a natural geometric structure on Θ : the geodesic distance between θ and θ' measures how different these parameter points are in terms of their influence on the model's predictions, rather than just their Euclidean distance.

For a parameterized model and its associated FIM, we consider the volume element induced by $\mathcal{F}(\theta)$:

$$dV(\theta) = \sqrt{\det(\mathcal{F}(\theta))} d\theta^1 \dots d\theta^d. \quad (\text{A1})$$

A geodesic ball $B(\theta, \epsilon)$ of radius ϵ centered at θ has volume

$$V(\theta, \epsilon) = \int_{B(\theta, \epsilon)} dV(\theta') = \int_{B(\theta, \epsilon)} \sqrt{\det(\mathcal{F}(\theta'))} d\theta'. \quad (\text{A2})$$

If $\sqrt{\det(\mathcal{F}(\theta))}$ is bounded by a positive constant $m > 0$, then for small ϵ , we can approximate:

$$V(\theta, \epsilon) \approx V_d \epsilon^d \sqrt{\det(\mathcal{F}(\theta))} \geq V_d \epsilon^d m, \quad (\text{A3})$$

where

$$V_d = \frac{\pi^{d/2}}{\Gamma(\frac{d}{2} + 1)}$$

is the volume of the unit ball in \mathbb{R}^d . Intuitively, a lower bound on $\sqrt{\det(\mathcal{F}(\theta))}$ ensures that geodesic balls are not “too small,” implying fewer truly distinct parameter configurations at ϵ . This geometric insight underpins the covering number bound we discuss next.

A.2 Covering Numbers of a Parameter Space

The covering number of a parameter space Θ measures how many balls of radius ϵ are required to cover the entire space. Since the FIM provides a natural measure of distinguishability, a lower bound on $\sqrt{\det(\mathcal{F}(\theta))}$ relates volumes of small balls to parameter distinguishability.

Lemma A.1 (Covering Number and Volume). *Let $\Theta \subset \mathbb{R}^d$ be a compact parameter space with volume V_Θ . Assume that the determinant of the Fisher Information Matrix $\mathcal{F}(\theta)$ satisfies:*

$$\sqrt{\det(\mathcal{F}(\theta))} \geq m > 0, \quad \forall \theta \in \Theta.$$

Then, for any $\epsilon > 0$, the covering number $N(\epsilon, \Theta, \|\cdot\|)$ of Θ with respect to the Euclidean norm $\|\cdot\|$ satisfies:

$$\log N(\epsilon, \Theta, \|\cdot\|) \leq C - d \log \epsilon, \tag{A4}$$

where $C = \log V_\Theta - \log V_d - \log m$ and $V_d = \frac{\pi^{\frac{d}{2}}}{\Gamma(\frac{d}{2}+1)}$ is the volume of a unit ball in \mathbb{R}^d .

Proof. Consider an ϵ -ball around θ :

$$V(\theta, \epsilon) \geq V_d \epsilon^d m.$$

To cover Θ , the total volume of N such balls must be at least V_Θ . So we have:

$$N(\epsilon, \Theta, \|\cdot\|) \leq \frac{V_\Theta}{V_d \epsilon^d m}. \tag{A5}$$

Taking the logarithm:

$$\begin{aligned} \log N(\epsilon, \Theta, \|\cdot\|) &\leq \log V_\Theta - \log (V_d \epsilon^d m) \\ &= \log V_\Theta - \log V_d - \log m - d \log \epsilon \\ &= C - d \log \epsilon. \end{aligned}$$

This completes the proof of lemma (A.1). □

The inequality (A4) shows how covering numbers scale with dimension d and resolution ϵ . Smaller ϵ or larger d requires more balls, thus more complex model classes. Conversely, a larger m reduces complexity by ensuring a certain “geometric rigidity” in the parameter space.

Appendix B

B.1 Bounding Empirical Rademacher Complexity

We now relate covering numbers to the empirical Rademacher complexity $\hat{\mathcal{R}}_N(\mathcal{F}_\Theta)$ of the model class $\mathcal{F}_\Theta = \{f_{\theta,p} : \theta \in \Theta\}$. The Rademacher complexity quantifies the model's capacity to fit random noise and thus provides an upper bound on generalization error.

Lemma B.1 (Empirical Rademacher Complexity Bound). *Let $\mathcal{F}_\Theta = \{f_{\theta,p} : \theta \in \Theta\}$ be a model function class. Let $\mathcal{D} = \{x_i, y_i\}_{i=1}^N$ be a dataset of N samples drawn from the distribution P . Assume that $f_{\theta,p}$ is bounded by the Lipschitz constant L_f^p and the determinant of the quantum Fisher information matrix is at least m . Then the empirical Rademacher complexity of the model class \mathcal{F}_Θ is bounded by:*

$$\hat{\mathcal{R}}_N(\mathcal{F}_\Theta) \leq \frac{6\sqrt{\pi d} \exp\left(\frac{C'}{d}\right)}{\sqrt{N}} \quad (\text{B6})$$

where $C' = \log V_\Theta - \log V_d - \log m + d \log L_f^p$.

Proof. Given a dataset $\mathcal{D} = \{x_i, y_i\}_{i=1}^N$ the empirical Rademacher complexity of a model class \mathcal{F}_Θ is defined as:

$$\hat{\mathcal{R}}_N(\mathcal{F}_\Theta) = \mathbb{E}_\sigma \left[\sup_{f \in \mathcal{F}_\Theta} \sum_{i=1}^N \sigma_i f(x_i) \right], \quad (\text{B7})$$

where $\sigma = \{\sigma_i\}_{i=1}^N$ are i.i.d Rademacher random variables, taking values in $\{-1, +1\}$ with equal probabilities. Dudley's entropy integral provides an upper bound on the empirical Rademacher complexity in terms of the covering numbers. If we let $\|\cdot\|_{2,\mathcal{D}}$ be the empirical L_2 -norm over the sample \mathcal{D} , we have:

$$\hat{\mathcal{R}}_N(\mathcal{F}_\Theta) \leq \frac{12}{\sqrt{N}} \int_0^{\epsilon_{max}} \sqrt{\log N(\epsilon, \mathcal{F}_\Theta, \|\cdot\|_{2,\mathcal{D}})} d\epsilon. \quad (\text{B8})$$

where $N(\epsilon, \mathcal{F}_\Theta, \|\cdot\|_{2,\mathcal{D}})$ is the covering number of \mathcal{F}_Θ with respect empirical L_2 metric:

$\|f - g\|_{2,\mathcal{D}} = \left(\frac{1}{N} \sum_{i=1}^N (f(x_i) - g(x_i))^2 \right)^{\frac{1}{2}}$ and $\epsilon_{max} = \sup_{f \in \mathcal{F}_\Theta} \|f\|_{2,\mathcal{D}}$. Since $f_{\theta,p}$ is bounded by the Lipschitz constant L_f^p , we can write: $\|f_{\theta,p} - f_{\theta',p}\|_{2,\mathcal{D}} \leq L_f^p \|\theta - \theta'\|$, $\forall \theta, \theta' \in \Theta$. This implies that an ϵ -cover of Θ with respect to the Euclidean norm $\|\cdot\|$ is also an ϵL_f^p -cover of \mathcal{F}_Θ with respect to the empirical L_2 metric. Using Lemma A.1, we can write:

$$\begin{aligned} \log N(\epsilon, \mathcal{F}_\Theta, \|\cdot\|_{2,\mathcal{D}}) &\leq \log N\left(\frac{\epsilon}{L_f^p}, \Theta, \|\cdot\|\right) \\ &\leq C - d \log\left(\frac{\epsilon}{L_f^p}\right) = C - d(\log \epsilon - \log L_f^p) \end{aligned}$$

$$\implies \log N(\epsilon, \mathcal{F}_\Theta, \|\cdot\|_{2, \mathcal{D}}) \leq C' - d \log \epsilon, \quad (\text{B9})$$

Substituting this result into equation (B8) gives:

$$\hat{R}_N(\mathcal{F}_\Theta) \leq \frac{12}{\sqrt{N}} \int_0^{\epsilon_{max}} \sqrt{C' - d \log \epsilon} d\epsilon. \quad (\text{B10})$$

We perform the elementary calculus in the following derivations and if the reader trusts our calculations, they may skip the following steps.

Let $t = -\log \epsilon$, so $\epsilon = e^{-t}$ and $d\epsilon = -e^{-t} dt$. The limit changes as: when $\epsilon = \epsilon_{max}$, $t = \log \epsilon_{max}$ and as ϵ decreases from ϵ_{max} to 0, t increases from $-\log \epsilon_{max}$ to 0. Thus:

$$\hat{R}_N(\mathcal{F}_\Theta) \leq \frac{12}{\sqrt{N}} \int_{-\log \epsilon_{max}}^0 \sqrt{C' - d \log e^{-t}} - e^{-t} dt$$

Assuming $\epsilon_{max} = 1$ (since $f_{\theta,p}(x)$ is bounded in $[0,1]$), we have $t = 0$ at $\epsilon = 1$, so:

$$\hat{R}_N(\mathcal{F}_\Theta) \leq \frac{12}{\sqrt{N}} \int_0^\infty \sqrt{C' + dt} e^{-t} dt$$

To make the derivation easier let us define:

$$I = \int_0^\infty \sqrt{C' + dt} e^{-t} dt \quad (\text{B11})$$

Let $S = C' + dt$, then $t = \frac{S-C'}{d}$ and $\frac{dt}{dS} = \frac{d}{dS} \left(\frac{S-C'}{d} \right) \implies dt = \frac{dS}{d}$ and $e^{-t} = e^{-\left(\frac{S-C'}{d}\right)} = e^{\frac{C'}{d}} e^{-\frac{S}{d}}$. Since, C' and d are constants, we can write:

$$I = \int_{C'}^\infty \sqrt{S} e^{\frac{C'}{d}} e^{-\frac{S}{d}} \frac{dS}{d} = \frac{e^{\frac{C'}{d}}}{d} \int_{C'}^\infty \sqrt{S} e^{-\frac{S}{d}} dS$$

Let $u = \frac{s}{d} \implies s = du$ and $ds = ddu$. Thus,

$$I = \frac{e^{\frac{C'}{d}}}{d} \int_{\frac{C'}{d}}^\infty \sqrt{du} e^{-u} d(du) = e^{\frac{C'}{d}} \sqrt{d} \int_{\frac{C'}{d}}^\infty u^{\frac{1}{2}} e^{-u} du$$

This integral is the gamma function and can be written as: $I = e^{\frac{C'}{d}} \sqrt{d} \Gamma\left(\frac{3}{2}, \frac{C'}{d}\right)$. Since $\Gamma(s, a) \leq \Gamma(s)$ for $a > 0$, and $\Gamma\left(\frac{3}{2}\right) = \frac{\sqrt{\pi}}{2}$ we can write:

$$I \leq e^{\frac{C'}{d}} \sqrt{d} \frac{\sqrt{\pi}}{2} \quad (\text{B12})$$

Substituting this back into equation (B8), we get:

$$\hat{\mathcal{R}}_N(\mathcal{F}_\Theta) \leq \frac{6\sqrt{\pi d} e^{\left(\frac{C'}{d}\right)}}{\sqrt{n}} \quad (\text{B13})$$

This completes the proof of the lemma (B.1). \square

This lemma encapsulates how geometry (via quantum FIM) and parameter space volume control Rademacher complexity. As N grows, the complexity term diminishes, indicating improved generalization potential.

Next, we discuss how the Rademacher complexity bound can be used to derive a generalization bound for quantum machine learning models.

B.2 Generalization Bound

We now derive the generalization bound proposed in Theorem 5.1 in the main text. The bound follows from standard statistical learning theory and the Rademacher complexity result obtained above.

Theorem B.2 (Restatement of Theorem 5.1). *Let $d, N \in \mathbb{N}, \delta \in (0, 1)$, and consider a parameter space $\Theta \subset \mathbb{R}^d$. The quantum model class $\mathcal{F}_\Theta = \{f_\theta, p : \theta \in \Theta\}$ with noise parameter $p \in [0, 1]$ satisfies $f_{\theta,p}(x) = \eta(p)f_\theta(x)$ with $\eta(0) = 1$. Assume:*

- The loss $l : \mathcal{Y} \times \mathbb{R} \rightarrow [0, 1]$ is Lipschitz continuous in its second argument with constant $L \leq 1$.
- The model gradients are bounded as: $\|\nabla_\theta f_{\theta,p}(x)\| \leq L_f^p$.
- The quantum FIM satisfies $\sqrt{\det(\mathcal{F}(\theta))} \geq m > 0$.

Define $C' = \log V_\Theta - \log V_d - \log m + d \log L_f^p$.

Then with probability at least $1 - \delta$ over an i.i.d. sample $D = \{x_i, y_i\}_{i=1}^N$ of size N ,

$$R(\theta) \leq \hat{R}_N(\theta) + \frac{12\sqrt{\pi d} \exp(C'/d)}{\sqrt{N}} + 3\sqrt{\frac{\log(2/\delta)}{2N}}, \quad (\text{B14})$$

uniformly for all $\theta \in \Theta$.

Proof. A standard result in learning theory states that with probability at least $1 - \delta$:

$$R(\theta) \leq \hat{R}_N(\theta) + 2\hat{\mathcal{R}}_N(\mathcal{L}) + 3\sqrt{\frac{\log(2/\delta)}{2N}}, \quad (\text{B15})$$

where $\mathcal{L} = \{(x, y) \mapsto l(y, f_{\theta,p}(x)) : \theta \in \Theta\}$.

Since $l(y, \hat{y})$ is Lipschitz with constant L and $f_{\theta,p}(x)$ is bounded by L_f^p , it follows that \mathcal{L} has Rademacher complexity at most $L \cdot L_f^p$. Applying Lemma B.1:

$$\hat{\mathcal{R}}_N(\mathcal{L}) \leq LL_f^p \frac{6\sqrt{\pi d} \exp(C'/d)}{\sqrt{N}}.$$

For $L \leq 1$, this simplifies directly to:

$$\hat{\mathcal{R}}_N(\mathcal{L}) \leq \frac{6\sqrt{\pi d} \exp(C'/d)}{\sqrt{N}}.$$

Substitute back into the generalization inequality:

$$R(\theta) \leq \hat{R}_N(\theta) + 2 \cdot \frac{6\sqrt{\pi d} \exp(C'/d)}{\sqrt{N}} + 3\sqrt{\frac{\log(2/\delta)}{2N}}.$$

This gives:

$$R(\theta) \leq \hat{R}_N(\theta) + \frac{12\sqrt{\pi d} \exp(C'/d)}{\sqrt{N}} + 3\sqrt{\frac{\log(2/\delta)}{2N}},$$

matching the statement of Theorem 5.1. \square

This completes the proof of the generalization bound for theorem 5.1. The interplay between Fisher information geometry, covering numbers, and Rademacher complexity provides a path from parameter space properties to explicit generalization guarantees. In practice, after training, restricting to local regions or reducing dimension to the effective dimension often yields sharper bounds.

References

- [1] Schuld, M., Petruccione, F.: Machine Learning with Quantum Computers, 2nd edn. Quantum Science and Technology. Springer, Cham, Switzerland (2021). <https://doi.org/10.1007/978-3-030-83098-4>
- [2] Biamonte, J., Wittek, P., Pancotti, N., Rebentrost, P., Wiebe, N., Lloyd, S.: Quantum machine learning. *Nature* **549**(7671), 195–202 (2017)
- [3] Wang, Y., Liu, J.: A comprehensive review of quantum machine learning: from nisq to fault tolerance. arXiv preprint arXiv:2401.11351 (2024)
- [4] Preskill, J.: Quantum computing in the nisq era and beyond. *Quantum* **2**, 79 (2018)
- [5] Torlai, G., Melko, R.G.: Machine-learning quantum states in the nisq era. *Annual Review of Condensed Matter Physics* **11**(1), 325–344 (2020)
- [6] Khanal, B., Rivas, P., Sanjel, A., Sooksatra, K., Quevedo, E., Rodriguez, A.: Generalization error bound for quantum machine learning in nisq era—a survey. *Quantum Machine Intelligence* **6**(2), 1–20 (2024)

- [7] Havlíček, V., Córcoles, A.D., Temme, K., Harrow, A.W., Kandala, A., Chow, J.M., Gambetta, J.M.: Supervised learning with quantum-enhanced feature spaces. *Nature* **567**(7747), 209–212 (2019)
- [8] Cerezo, M., Arrasmith, A., Babbush, R., Benjamin, S.C., Endo, S., Fujii, K., McClean, J.R., Mitarai, K., Yuan, X., Cincio, L., *et al.*: Variational quantum algorithms. *Nature Reviews Physics* **3**(9), 625–644 (2021)
- [9] Lloyd, S., Rebentrost, P., Mohseni, M.: Quantum algorithms for supervised and unsupervised machine learning. arXiv preprint arXiv:1307.0411 (2013)
- [10] Aïmeur, E., Brassard, G., Gambs, S.: Quantum clustering algorithms. In: Proceedings of the 24th International Conference on Machine Learning, pp. 1–8 (2007)
- [11] Mohri, M., Rostamizadeh, A., Talwalkar, A.: Foundations of Machine Learning, (2018). Second Edition. <https://mitpress.ubliish.com/ebook/foundations-of-machine-learning-2-preview/7093/Cover>
- [12] Abu-Mostafa, Y.S., Magdon-Ismail, M., Lin, H.T.: Learning from data: A short course (2012)
- [13] Shalev-Shwartz, S., Ben-David, S.: Understanding machine learning: From theory to algorithms (2014)
- [14] Emami, M., Sahraee-Ardakan, M., Pandit, P., Rangan, S., Fletcher, A.: Generalization error of generalized linear models in high dimensions. In: International Conference on Machine Learning, pp. 2892–2901 (2020). PMLR
- [15] Jakubovitz, D., Giryes, R., Rodrigues, M.R.: Generalization error in deep learning. In: Compressed Sensing and Its Applications: Third International MATHEON Conference 2017, pp. 153–193 (2019). Springer
- [16] Nadeau, C., Bengio, Y.: Inference for the generalization error. *Advances in neural information processing systems* **12** (1999)
- [17] Banchi, L., Pereira, J., Pirandola, S.: Generalization in quantum machine learning: A quantum information standpoint. *PRX Quantum* **2**(4), 040321 (2021)
- [18] Gil-Fuster, E., Eisert, J., Bravo-Prieto, C.: Understanding quantum machine learning also requires rethinking generalization. arXiv preprint arXiv:2306.13461 (2023)
- [19] Caro, M.C., Gil-Fuster, E., Meyer, J.J., Eisert, J., Sweke, R.: Encoding-dependent generalization bounds for parametrized quantum circuits. *Quantum* **5**, 582 (2021)
- [20] Khanal, B., Rivas, P.: Evaluating the impact of noise on variational quantum circuits in nisq era devices. In: 2023 Congress in Computer Science, Computer

Engineering, & Applied Computing (CSCE) (2023)

- [21] Caro, M.C., Huang, H.-Y., Cerezo, M., Sharma, K., Sornborger, A., Cincio, L., Coles, P.J.: Generalization in quantum machine learning from few training data. *Nature communications* **13**(1), 4919 (2022)
- [22] Caro, M.C., Gur, T., Rouzé, C., Franca, D.S., Subramanian, S.: Information-theoretic generalization bounds for learning from quantum data. In: *The Thirty Seventh Annual Conference on Learning Theory*, pp. 775–839 (2024). PMLR
- [23] Haug, T., Kim, M.: Generalization with quantum geometry for learning unitaries. *arXiv preprint arXiv:2303.13462* (2023)
- [24] Canatar, A., Peters, E., Pehlevan, C., Wild, S.M., Shaydulin, R.: Bandwidth enables generalization in quantum kernel models. *arXiv preprint arXiv:2206.06686* (2022)
- [25] Caro, M.C., Huang, H.-Y., Ezzell, N., Gibbs, J., Sornborger, A.T., Cincio, L., Coles, P.J., Holmes, Z.: Out-of-distribution generalization for learning quantum dynamics. *Nature Communications* **14**(1), 3751 (2023)
- [26] Abbas, A., Sutter, D., Zoufal, C., Lucchi, A., Figalli, A., Woerner, S.: The power of quantum neural networks. *Nature Computational Science* **1**(6), 403–409 (2021)
- [27] Hur, T., Park, D.K.: Understanding generalization in quantum machine learning with margins. *arXiv preprint arXiv:2411.06919* (2024)
- [28] Martinis, J.M., Nam, S., Aumentado, J., Lang, K., Urbina, C.: Decoherence of a superconducting qubit due to bias noise. *Physical Review B* **67**(9), 094510 (2003)
- [29] Wang, S., Fontana, E., Cerezo, M., Sharma, K., Sone, A., Cincio, L., Coles, P.J.: Noise-induced barren plateaus in variational quantum algorithms. *Nature communications* **12**(1), 6961 (2021)
- [30] Heyraud, V., Li, Z., Denis, Z., Le Boité, A., Ciuti, C.: Noisy quantum kernel machines. *Physical Review A* **106**(5), 052421 (2022)
- [31] Shor, P.W.: Scheme for reducing decoherence in quantum computer memory. *Physical review A* **52**(4), 2493 (1995)
- [32] Khanal, B., Rivas, P.: Learning robust observable to address noise in quantum machine learning. *arXiv preprint arXiv:2409.07632* (2024)
- [33] Shaib, A., Naim, M.H., Fouda, M.E., Kanj, R., Kurdahi, F.: Efficient noise mitigation technique for quantum computing. *Scientific Reports* **13**(1), 3912 (2023)
- [34] Ferracin, S., Hashim, A., Ville, J.-L., Naik, R., Carignan-Dugas, A., Qassim, H.,

- Morvan, A., Santiago, D.I., Siddiqi, I., Wallman, J.J.: Efficiently improving the performance of noisy quantum computers. *Quantum* **8**, 1410 (2024)
- [35] Qi, J., Yang, C.-H.H., Chen, P.-Y., Hsieh, M.-H.: Theoretical error performance analysis for variational quantum circuit based functional regression. *npj Quantum Information* **9**(1), 4 (2023)
- [36] Huang, H.-Y., Broughton, M., Mohseni, M., Babbush, R., Boixo, S., Neven, H., McClean, J.R.: Power of data in quantum machine learning. *Nature communications* **12**(1), 2631 (2021)
- [37] Liu, Y., Arunachalam, S., Temme, K.: A rigorous and robust quantum speed-up in supervised machine learning. *Nature Physics* **17**(9), 1013–1017 (2021)
- [38] Du, Y., Tu, Z., Yuan, X., Tao, D.: Efficient measure for the expressivity of variational quantum algorithms. *Physical Review Letters* **128**(8), 080506 (2022)
- [39] Gentinetta, G., Thomsen, A., Sutter, D., Woerner, S.: The complexity of quantum support vector machines. *Quantum* **8**, 1225 (2024)
- [40] Kübler, J., Buchholz, S., Schölkopf, B.: The inductive bias of quantum kernels. *Advances in Neural Information Processing Systems* **34**, 12661–12673 (2021)
- [41] Thanasilp, S., Wang, S., Cerezo, M., Holmes, Z.: Exponential concentration in quantum kernel methods. *Nature Communications* **15**(1), 5200 (2024)
- [42] Czarnik, P., Arrasmith, A., Coles, P.J., Cincio, L.: Error mitigation with clifford quantum-circuit data. *Quantum* **5**, 592 (2021)
- [43] Cerezo, M., Verdon, G., Huang, H.-Y., Cincio, L., Coles, P.J.: Challenges and opportunities in quantum machine learning. *Nature Computational Science* **2**(9), 567–576 (2022)
- [44] Holmes, Z., Sharma, K., Cerezo, M., Coles, P.J.: Connecting ansatz expressibility to gradient magnitudes and barren plateaus. *PRX Quantum* **3**(1), 010313 (2022)
- [45] Zhao, C., Gao, X.-S.: Analyzing the barren plateau phenomenon in training quantum neural networks with the zx-calculus. *Quantum* **5**, 466 (2021)
- [46] McClean, J.R., Boixo, S., Smelyanskiy, V.N., Babbush, R., Neven, H.: Barren plateaus in quantum neural network training landscapes. *Nature communications* **9**(1), 4812 (2018)
- [47] Arrasmith, A., Cerezo, M., Czarnik, P., Cincio, L., Coles, P.J.: Effect of barren plateaus on gradient-free optimization. *Quantum* **5**, 558 (2021)
- [48] Nielsen, M.A., Chuang, I.: *Quantum computation and quantum information*. American Association of Physics Teachers (2002)

- [49] Shalev-Shwartz, S., Shamir, O., Srebro, N., Sridharan, K.: Learnability, stability and uniform convergence. *The Journal of Machine Learning Research* **11**, 2635–2670 (2010)
- [50] Valle-Pérez, G., Louis, A.A.: Generalization bounds for deep learning. arXiv preprint arXiv:2012.04115 (2020)
- [51] Johansson, F.D., Shalit, U., Kallus, N., Sontag, D.: Generalization bounds and representation learning for estimation of potential outcomes and causal effects. *Journal of Machine Learning Research* **23**(166), 1–50 (2022)
- [52] Pape, A.D., Kurtz, K.J., Sayama, H.: Complexity measures and concept learning. *Journal of Mathematical Psychology* **64**, 66–75 (2015)
- [53] Bialek, W., Nemenman, I., Tishby, N.: Predictability, complexity, and learning. *Neural computation* **13**(11), 2409–2463 (2001)
- [54] Benedetti, M., Lloyd, E., Sack, S., Fiorentini, M.: Parameterized quantum circuits as machine learning models. *Quantum Science and Technology* **4**(4), 043001 (2019)
- [55] Holevo, A.S.: *Quantum Systems, Channels, Information: a Mathematical Introduction*. Walter de Gruyter GmbH & Co KG, ??? (2019)
- [56] Guță, M., Kahn, J.: Local asymptotic normality for qubit states. *Physical Review A—Atomic, Molecular, and Optical Physics* **73**(5), 052108 (2006)
- [57] Magesan, E., Gambetta, J.M., Emerson, J.: Scalable and robust randomized benchmarking of quantum processes. *Physical review letters* **106**(18), 180504 (2011)
- [58] Preskill, J.: *Lecture notes for physics 229: Quantum information and computation*. California institute of technology **16**(1), 1–8 (1998)
- [59] Khanal, B., Rivas, P.: A modified depolarization approach for efficient quantum machine learning. *Mathematics* **12**(9), 1385 (2024)
- [60] Haug, T., Kim, M.: Generalization of quantum machine learning models using quantum fisher information metric. *Physical Review Letters* **133**(5), 050603 (2024)
- [61] Kasatkin, V., Mozgunov, E., Ezzell, N., Lidar, D.: Detecting quantum and classical phase transitions via unsupervised machine learning of the fisher information metric. arXiv preprint arXiv:2408.03418 (2024)
- [62] Bharti, K.: Fisher information: A crucial tool for nisq research. *Quantum Views* **5**, 61 (2021)

- [63] Meyer, J.J.: Fisher information in noisy intermediate-scale quantum applications. *Quantum* **5**, 539 (2021)
- [64] Amari, S.-I.: Natural gradient works efficiently in learning. *Neural computation* **10**(2), 251–276 (1998)
- [65] Haug, T., Bharti, K., Kim, M.: Capacity and quantum geometry of parametrized quantum circuits. *PRX Quantum* **2**(4), 040309 (2021)
- [66] Martens, J.: New insights and perspectives on the natural gradient method. *Journal of Machine Learning Research* **21**(146), 1–76 (2020)
- [67] Stokes, J., Izaac, J., Killoran, N., Carleo, G.: Quantum natural gradient. *Quantum* **4**, 269 (2020)
- [68] Baumgratz, T., Nüßeler, A., Cramer, M., Plenio, M.B.: A scalable maximum likelihood method for quantum state tomography. *New Journal of Physics* **15**(12), 125004 (2013)
- [69] Braunstein, S.L., Caves, C.M.: Statistical distance and the geometry of quantum states. *Physical Review Letters* **72**(22), 3439 (1994)
- [70] Liu, J., Yuan, H., Lu, X.-M., Wang, X.: Quantum fisher information matrix and multiparameter estimation. *Journal of Physics A: Mathematical and Theoretical* **53**(2), 023001 (2020)
- [71] Fujiwara, A.: Quantum channel identification problem. *Physical Review A* **63**(4), 042304 (2001)
- [72] Petz, D., Ghinea, C.: Introduction to quantum fisher information. In: *Quantum Probability and Related Topics*, pp. 261–281. World Scientific, ??? (2011)
- [73] Yamamoto, N.: On the natural gradient for variational quantum eigensolver. arXiv preprint arXiv:1909.05074 (2019)
- [74] Liu, J., Xiong, H.-N., Song, F., Wang, X.: Fidelity susceptibility and quantum fisher information for density operators with arbitrary ranks. *Physica A: Statistical Mechanics and its Applications* **410**, 167–173 (2014)
- [75] Abbas, A., Sutter, D., Figalli, A., Woerner, S.: Effective dimension of machine learning models. arXiv preprint arXiv:2112.04807 (2021)
- [76] Schuld, M., Sweke, R., Meyer, J.J.: Effect of data encoding on the expressive power of variational quantum-machine-learning models. *Physical Review A* **103**(3), 032430 (2021)
- [77] Vapnik, V.: *Statistical learning theory*. John Wiley & Sons google schola **2**, 831–842 (1998)

- [78] Helstrom, C.W.: Quantum detection and estimation theory. *Journal of Statistical Physics* **1**, 231–252 (1969)
- [79] Paris, M.G.: Quantum estimation for quantum technology. *International Journal of Quantum Information* **7**(supp01), 125–137 (2009)
- [80] Bartlett, P.L., Mendelson, S.: Rademacher and gaussian complexities: Risk bounds and structural results. *Journal of Machine Learning Research* **3**(Nov), 463–482 (2002)
- [81] Larocca, M., Ju, N., García-Martín, D., Coles, P.J., Cerezo, M.: Theory of overparametrization in quantum neural networks. *Nature Computational Science* **3**(6), 542–551 (2023)
- [82] Ciliberto, C., Herbster, M., Ialongo, A.D., Pontil, M., Rocchetto, A., Severini, S., Wossnig, L.: Quantum machine learning: a classical perspective. *Proceedings of the Royal Society A: Mathematical, Physical and Engineering Sciences* **474**(2209), 20170551 (2018)
- [83] Schuld, M., Killoran, N.: Quantum machine learning in feature hilbert spaces. *Physical review letters* **122**(4), 040504 (2019)